5/8/1988

# The speed of axial propagation of a cylindrical bubble through a cylindrical vortex

Karim Shariff
NASA Ames Research Center, Moffett Field, CA 94035

October 25, 2001

**Abstract**

Inspired by the rapid elongation of air columns injected into vortices by dolphins, we present an exact inviscid solution for the axial speed (assumed steady) of propagation of the tip of a semi-infinite cylindrical bubble along the axis of a cylindrical vortex. The bubble is assumed to be held at constant pressure by being connected to a reservoir, the lungs of the dolphin, say. For a given bubble pressure, there is a modest critical rotation rate above which steadily propagating bubbles exist. For a bubble at ambient pressure, the propagation speed of the bubble (relative to axial velocity within the vortex) varies between 0.5 and 0.6 of the maximum rotational speed of the vortex. Surprisingly, the bubble tip can propagate (almost as rapidly) even when the pressure minimum in the vortex core is greater than the bubble pressure; in this case, solutions exhibit a dimple on the nose of the bubble. A situation important for incipient vortex cavitation, and one which dolphins also demonstrate, is elongation of a free bubble, i.e., one whose internal pressure may vary. Under the assumption that the acceleration term is small (checked *a posteriori*), the steady solution is applied at each instant during the elongation. Three types of behavior are then possible depending on physical parameters and initial conditions: (A) Unabated elongation with slowly increasing bubble pressure, and nearly constant volume. Volume begins to decrease in the late stages. (B1) Elongation with decreasing bubble pressure. A limit point of the steady solution is encountered at a finite bubble length. (B2) Unabated elongation with decreasing bubble pressure and indefinite creation of volume. This is made possible by the existence of propagating solutions at bubble pressures below the minimum vortex pressure. As the bubble stretches, its radius initially decreases but then becomes constant; this is also observed in experiments on incipient vortex cavitation.

# 1 Introduction

Marten *et al.* [1] report captive dolphins making bubbles interact with vortices in a number of ways. This behavior is performed, apparently for play, without any training or food reward, and at the dolphins' own volition.

In one case, the dolphins make ring vortices with a flick of their tail fins and then turn around to inject air into them from their blowholes. The air forms a tubular bubble that lengthens rapidly along the vortex core, eventually forming a toroidal bubble; see photographs at the top of pp. 86–87 in Marten *et al.* [1]. Dolphins also inject air into the longitudinal vortices created behind their dorsal fin. This too forms a cylindrical air column that rapidly propagates along the vortex; see figure 1. This situation differs from the case of the vortex ring in that axial flow is present in the vortex. In both of these examples, the bubble remains connected to the dolphin's blowhole or mouth while undergoing substantial increase in length. Hence we shall initially assume that the bubble pressure equals the reservoir pressure, which in turn is taken to be constant in time.

The mechanism for propagation of the bubble is simply that the lower than ambient pressure in the vortex core sucks the air, provided the surface tension is not too high. To see this mathematically, consider figure 2 which shows one end of the bubble propagating into the vortex. The bubble is assumed to be sufficiently long that there exists a region (station 2 in figure 2) where axial derivatives may be neglected; this is made more precise in §4. In order to the make the flow steady between stations 1 and 2, choose a reference frame that moves with the speed $U_\mathrm{b}$ of the bubble nose. Constancy of Bernoulli head along the axis streamline implies that the pressure at the tip of the nose is $p_\mathrm{n} = p_\mathrm{a} + \rho(U - U_\mathrm{b})^2/2$, where $p_\mathrm{a}$ is the pressure at the axis of the undisturbed vortex, $\rho$ is the liquid density, and $U$ is the axial velocity of the liquid at the vortex axis in the laboratory frame. Combining this with the pressure matching condition $p_\mathrm{b} - p_\mathrm{n} = \kappa T$ gives the bubble speed:

$$U_\mathrm{b} = U \pm \sqrt{2(p_\mathrm{b} - p_\mathrm{a} - T\kappa)}, \tag{1}$$

where $T$ is the surface tension and $\kappa$ is the total curvature at the tip. The $\pm$ symbol means that the tip may either advance through the vortex or retract. We shall choose the physically observed advancing solution; in reality it is presumably the initial condition that sets up the elongation. The speed would be determined by (1) if only $\kappa$ were known. In the present work, one is fortunate to be able to evaluate the speed without knowing $\kappa$, and in fact, to able to deduce $\kappa$ *a posteriori* using (1). What makes this evaluation possible is a useful method of analysis introduced by Batchelor [2] in which one matches two cylindrical

(axially invariant) solutions of the steady Euler equations at stations 1 and 2.

The case of a free bubble not connected to a reservoir and therefore having variable internal pressure is also important in three contexts:

(i) First, the dolphin stops blowing at some point.

(ii) Dolphins have also been observed to release free spherical bubbles and then to "whip them into shape" using vortices. For instance, one dolphin released a cloud of bubbles from its blowhole while swimming rapidly; the bubbles elongated into a long tube when they encountered the longitudinal vortex behind the dorsal fin; see photographs at the bottom of pp 86–87 in Marten *et al.* [1]. One observes a tremendous creation of volume from a few small bubbles. This may seem contrary to intuition for if the volume increases, the bubble pressure must at some instant fall below the vortex pressure, thus eliminating the driving mechanism for the elongation according to (1). The present solutions indicate that what permits elongation in this situation is $\kappa$ being $< 0$. Another dolphin stood upside down in the water and released a bubble from its mouth which rose towards the surface; when the bubble reached the tail fin, it was elongated into a ring vortex by a flick of the tail fin.

(iii) A similar phenomenon was observed in experiments on incipient vortex cavitation behind a wing tip conducted by Maines and Arndt [3]. They observed four stages: (I) Motion of a small spherical bubble towards the vortex axis driven by the radial pressure gradient in the vortex. This is also the reason why the bubble is initially helical in figure 1. (II): Volume expansion of the bubble in the shape of an ellipsoid whose major and minor axis both grow, with the major axis growing much more rapidly. (III) Explosive growth of the major axis accompanied by a decrease in minor axis. (IV) In the final phase, the bubble grows as a cylindrical bubble in which the length continues to increase while the radius becomes constant.

We shall provide a treatment in which the steady solution is applied to such situations under the assumption of quasi-steadiness.

# 2 Analysis

## 2.1 Bubble with specified pressure

We employ cylindrical coordinates $(x, \sigma, \phi)$ with corresponding velocity components $(u, v, w)$. The streamfunction $\psi(x, \sigma)$ defined by

$$u = \frac{1}{\sigma}\frac{\partial \psi}{\partial \sigma}, \qquad v = -\frac{1}{\sigma}\frac{\partial \psi}{\partial x}, \tag{2}$$

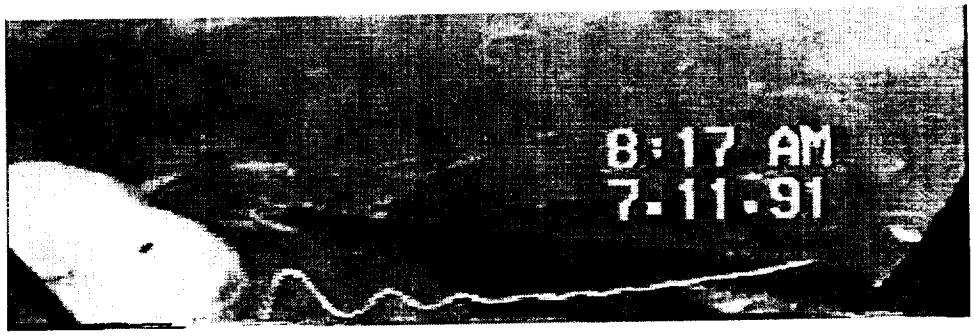


Figure 1: Dolphin injecting air into a vortex it previously created using its dorsal fin.

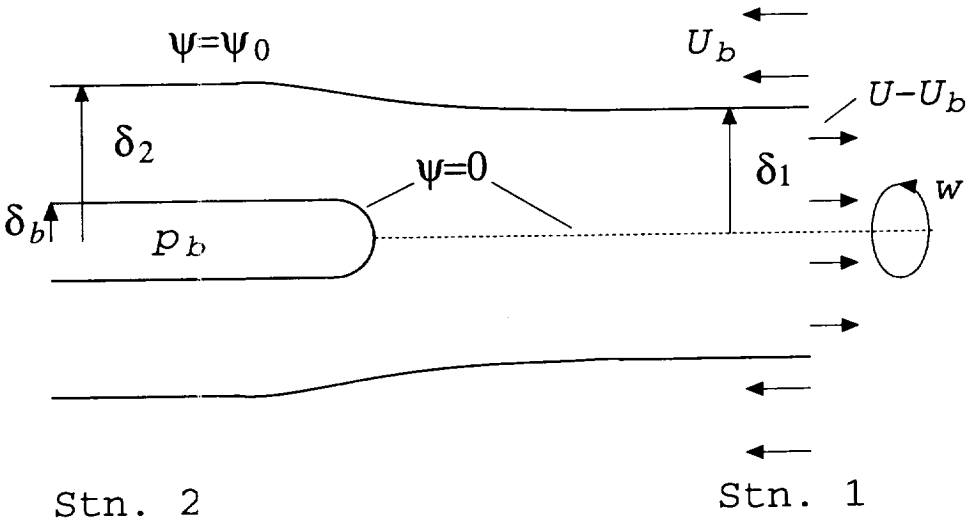


Figure 2: Sketch used for the analysis.

describes the flow in a meridional ($x\sigma$) plane. The swirling flow in the undisturbed vortex at station 1 is taken to be a Rankine vortex

$$w_1 = \begin{cases} \Omega\sigma, & \sigma \le \delta_1; \\ \Omega\delta_1^2/\sigma, & \sigma > \delta_1, \end{cases} \tag{3}$$

where $\delta_1$ is the vortex core size. The axial velocity in the undisturbed vortex is assumed to have a uniform axial velocity, $U$, such that in the reference frame moving with the bubble tip we have

$$u_1 = \begin{cases} U - U_\mathrm{b}, & \sigma \le \delta_1; \\ -U_\mathrm{b}, & \sigma > \delta_1. \end{cases} \tag{4}$$

These choices for the vortex flow were made for analytical tractability. More general profiles may be treated by the procedure below but it has to be implemented entirely using numerical analysis.

Steady axisymmetric inviscid flow is governed by the Squire-Long equation [2],

$$\frac{\partial^2\psi}{\partial x^2} + \frac{\partial^2\psi}{\partial\sigma^2} - \frac{1}{\sigma}\frac{\partial\psi}{\partial\sigma} = \sigma^2 H'(\psi)/\rho - K(\psi)K'(\psi), \tag{5}$$

where $K(\psi) = \sigma w$ is the circulation function and $H(\psi) = p + \rho|\mathbf{u}|^2/2$ is the Bernoulli head. We shall follow a very useful but simple method of analysis introduced by Batchelor [2] in which one joins two axially invariant solutions of (5) at two stations.

The first step is to obtain the functions $K(\psi)$ and $H(\psi)$ from the flow at station 1. At this location, the streamfunction obtained using (2) and (4) is:

$$\psi_1(\sigma) = \begin{cases} (U - U_\mathrm{b})\sigma^2/2, & \sigma < \delta_1; \\ (U\delta_1^2 - U_\mathrm{b}\sigma^2)/2, & \sigma \ge \delta_1. \end{cases} \tag{6}$$

For later use, let us define the streamfunction for the vortex boundary:

$$\psi_0 \equiv \psi_1(\delta_1) = (U - U_\mathrm{b})\,\delta_1^2/2. \tag{7}$$

After solving (6) for $\sigma^2$ in terms of $\psi$, the circulation function is obtained:

$$K(\psi) = \sigma w = \begin{cases} 2\psi\Omega/(U - U_\mathrm{b}), & \sigma \le \delta_1; \\ \Omega\delta_1^2, & \sigma > \delta_1. \end{cases} \tag{8}$$

The pressure at station 1, obtained after integrating

$$\frac{\partial p_1}{\partial\sigma} = \frac{\rho w_1^2}{\sigma}, \tag{9}$$

is

$$p_1 = \begin{cases} p_\infty + \rho\Omega^2\left(\sigma^2/2 - \delta_1^2\right), & \sigma < \delta_1; \\ p_\infty - \rho\Omega^2\delta_1^4/(2\sigma^2), & \sigma \geq \delta_1. \end{cases} \tag{10}$$

Evaluating $H(\psi) = p_1 + \rho|\mathbf{u}_1|^2/2$ and writing $\sigma$ in terms of $\psi$ gives

$$H(\psi) = \begin{cases} p_\infty + \rho\Omega^2\left(2\psi/(U - U_\mathrm{b}) - \delta_1^2\right) + \rho\left(U - U_\mathrm{b}\right)^2/2, & \text{within the vortex;} \\ p_\infty + \rho U_\mathrm{b}^2/2, & \text{outside the vortex.} \end{cases} \tag{11}$$

Inserting (8) and (11) into (5) gives for an axially invariant flow:

$$\frac{\partial^2\psi}{\partial\sigma^2} - \frac{1}{\sigma}\frac{\partial\psi}{\partial\sigma} = \frac{2\Omega^2}{(U - U_\mathrm{b})} \begin{cases} \sigma^2 - 2\psi/(U - U_\mathrm{b}), & \text{inside the vortex;} \\ 0, & \text{outside.} \end{cases} \tag{12}$$

We obtain $\psi$ at station 2 by solving (12). In the interior region, (12) has the same form as an equation obtained by Batchelor [2](p. 546) and we simply use his solution. In the exterior, we assume a solution of the form $\psi \propto \sigma^m$. The result is:

$$\psi_2(\sigma) = \begin{cases} -\left(U_\mathrm{b} - U\right)\sigma^2/2 + \sigma\left[AJ_1(k\sigma) + BY_1(k\sigma)\right], & \sigma < \delta_2; \\ -U_\mathrm{b}\sigma^2/2 + C, & \sigma \geq \delta_2, \end{cases} \tag{13}$$

where

$$k \equiv \frac{2\Omega}{(U - U_\mathrm{b})}. \tag{14}$$

The constant $C = (1/2)U\delta_1^2$ by imposing the condition that $\psi_2(\delta_2) = \psi_0$. The velocity corresponding to (13) is

$$u_2(\sigma) = \begin{cases} -\left(U_\mathrm{b} - U\right) + AkJ_0(k\sigma) + BkY_0(k\sigma), & \sigma < \delta_2; \\ -U_\mathrm{b}, & \sigma \geq \delta_2. \end{cases} \tag{15}$$

The five unknowns $U_\mathrm{b} - U, \delta_\mathrm{b}, \delta_2, A, B$ are obtained by imposing five conditions:

(1) The bubble surface must be a streamtube, i.e., $\psi_2(\delta_\mathrm{b}) = 0$:

$$-\frac{1}{2}\left(U_\mathrm{b} - U\right) + AJ_1(k\delta_\mathrm{b}) + BY_1(k\delta_\mathrm{b}) = 0. \tag{16}$$

(2) The vortex boundary must be the same streamsurface at stations 1 and 2, i.e., $\psi_2(\delta_2) = \psi_0$:

$$-\frac{1}{2}\left(U_\mathrm{b} - U\right)\delta_1^2 = -\frac{1}{2}\left(U_\mathrm{b} - U\right)\delta_2^2 + \delta_2\left[AJ_1(k\delta_2) + BY_1(k\delta_2)\right]. \tag{17}$$

(3) The pressure must be continuous at $\sigma = \delta_2$, i.e., $p_2(\sigma = \delta_2^-) = p_2(\sigma = \delta_2^+)$. The pressure, $p_2(\sigma = \delta_2^+)$, just outside the vortex is obtained by equating the value of the Bernoulli head in the exterior region to its definition:

$$p_\infty + \frac{1}{2}\rho U_\mathrm{b}^2 = p_2(\sigma = \delta_2^+) + \frac{1}{2}\rho\left[u_2^2(\delta_2^+) + w_2^2(\delta_2^+)\right]. \tag{18}$$

The pressure, $p_2(\delta_2^-)$, just inside the vortex is obtained by evaluating $H(\psi)$ of the inner region at $\psi = \psi_0$ and equating it to its definition:

$$p_\infty + \frac{1}{2}\rho\,(U_\mathrm{b} - U)^2 = p_2(\delta_2^-) + \frac{1}{2}\rho\left[u_2^2(\delta_2^-) + w_2^2(\delta_2^-)\right]. \tag{19}$$

Subtracting (19) from (18) and using the fact that both pressure and azimuthal velocity must be continuous gives

$$u_2(\delta_2^-) = \pm\,(U_\mathrm{b} - U) \tag{20}$$

To choose the correct sign in (20), one argues that in the case when the axial velocity in the vortex $U = 0$, a vortex sheet does not exist and therefore the axial velocity must be continuous, i.e. $u(\delta_2^-) = -U_\mathrm{b}$. Hence, we choose the minus sign in (20) and obtain:

$$AJ_0(k\delta_2) + BY_0(k\delta_2) = 0. \tag{21}$$

(4) Forces must balance on the bubble surface at station 2:

$$p_\mathrm{b} - p_2(\delta_\mathrm{b}) = T/\delta_\mathrm{b}. \tag{22}$$

The pressure $p_2(\delta_\mathrm{b})$ is obtained by equating the value of $H(\psi)$ at the bubble surface ($\psi = 0$) to its definition:

$$p_\infty - \rho\Omega^2\delta_1^2 + \frac{1}{2}\rho\,(U_\mathrm{b} - U)^2 = p_2(\delta_\mathrm{b}) + \frac{1}{2}\rho\left[u_2^2(\delta_\mathrm{b}) + w_2^2(\delta_\mathrm{b})\right]. \tag{23}$$

Solving (23) for $p_2(\delta_\mathrm{b})$, substituting this into (22), and noting that the azimuthal velocity $w(\delta_\mathrm{b})$ on the bubble surface vanishes because $K(\psi = 0) = 0$ gives:

$$p_\mathrm{b} - p_\infty - \frac{1}{2}\rho\,(U_\mathrm{b} - U)^2 + \rho\Omega^2\delta_1^2 + \frac{1}{2}\rho u_2^2(\delta_\mathrm{b}) - \frac{T}{\delta_\mathrm{b}} = 0, \tag{24}$$

where

$$u(\delta_\mathrm{b}) = -(U_\mathrm{b} - U) + AkJ_0(k\delta_\mathrm{b}) + BkY_0(k\delta_\mathrm{b}). \tag{25}$$

At this point, let us introduce non-dimensional quantities (denoted by hats) using the density $\rho$, vortex core radius $\delta_1$, and angular velocity $\Omega$ as the scaling quantities:

$$\begin{aligned} \widehat{A} &= \frac{A}{\Omega\delta_1^2}, \quad \widehat{B} = \frac{B}{\Omega\delta_1^2}, \quad \widehat{\delta}_\mathrm{b} = \frac{\delta_\mathrm{b}}{\delta_1}, \quad \widehat{\delta}_2 = \frac{\delta_2}{\delta_1}, \quad \Delta\widehat{U}_\mathrm{b} = \frac{U_\mathrm{b} - U}{\Omega\delta_1}, \\ \Delta\widehat{p}_\mathrm{b} &= \frac{p_\mathrm{b} - p_\infty}{\rho\Omega^2\delta_1^2}, \quad \widehat{T} = \frac{T}{\rho\Omega^2\delta_1^3}. \end{aligned} \tag{26}$$

An expression in dimensional form may be converted to non-dimensional form by setting $\rho$, $\delta_1$, and $\Omega$ to unity and placing hats over all quantities.

(5) The fifth condition is that axial momentum must balance in the region between stations 1 and 2:

$$2\pi T\delta_{\rm b} + 2\pi \int_0^\infty \sigma d\sigma \left[p_1(\sigma) + \rho u_1^2(\sigma) - p_2(\sigma) - \rho u_2^2(\sigma)\right] = 0 \tag{27}$$

Notice that $\int \rho uv\, \sigma dx$, the radial flux of axial momentum at the outer radial boundary $\sigma \to \infty$, does not appear in (27). This is because the radial velocity $v \sim \sigma^{-2}$ given that there are no sources of volume. When pressure and velocity profiles are substituted into (27), several integrals involving Bessel functions appear. These integrals are provided in Gradshteyn & Ryzhik [4] 5.54.2, 5.56.2, and Watson [5] p.134, eq. (10). The integrals were supplied to Mathematica which performed the rest of the algebra. The final result is:

$$T_1 + T_2 + T_3 = 0, \tag{28}$$

where

$$\begin{aligned}
T_1 &= -\frac{3}{8} + \frac{1}{2}\widehat{\delta}_2^2 - \frac{1}{2}\widehat{\delta}_{\rm b}^2 + \frac{1}{8}\widehat{\delta}_{\rm b}^4 - \frac{1}{8}\widehat{\delta}_2^4 - \frac{1}{2}\widehat{\delta}_{\rm b}^2\widehat{p}_{\rm b} + \widehat{\delta}_{\rm b}\widehat{T} + \frac{1}{2}\widehat{\delta}_{\rm b}^2\widehat{U}_{\rm b}^2 - \frac{1}{2}\log\left(\widehat{\delta}_2\right) \\
T_2 &= \frac{1}{\widehat{U}_{\rm b}^2}\left[\widehat{A}^2\left(\widehat{\delta}_{\rm b}^2 f_1 - \widehat{\delta}_2^2 f_2\right) + \widehat{A}\widehat{B}\left(\widehat{\delta}_{\rm b}^2 f_3 - \widehat{\delta}_2^2 f_4\right) + \widehat{B}^2\left(\widehat{\delta}_{\rm b}^2 f_5 - \widehat{\delta}_2^2 f_6\right)\right] \\
T_3 &= \widehat{U}_{\rm b}\left(\widehat{A} f_7 + \widehat{B} f_8\right)
\end{aligned}$$

with

$$\begin{aligned}
f_1 &= J_0^2(\eta_{\rm b}) + J_0(\eta_{\rm b})J_2(\eta_{\rm b}) \\
f_2 &= J_0^2(\eta_2) + J_0(\eta_2)J_2(\eta_2) \\
f_3 &= J_2(\eta_{\rm b})Y_0(\eta_{\rm b}) + 2J_0(\eta_{\rm b})Y_0(\eta_{\rm b}) + J_0(\eta_{\rm b})Y_2(\eta_{\rm b}) \\
f_4 &= 2J_0(\eta_2)Y_0(\eta_2) + J_2(\eta_2)Y_0(\eta_2) + J_0(\eta_2)Y_2(\eta_2) \\
f_5 &= Y_0^2(\eta_{\rm b}) + Y_0(\eta_{\rm b})Y_2(\eta_{\rm b}) \\
f_6 &= Y_0^2(\eta_2) + Y_0(\eta_2)Y_2(\eta_2) \\
f_7 &= \widehat{\delta}_2 J_1(\eta_2) - \widehat{\delta}_{\rm b} J_1(\eta_{\rm b}) \\
f_8 &= \widehat{\delta}_2 Y_1(\eta_2) - \widehat{\delta}_{\rm b} Y_1(\eta_{\rm b})
\end{aligned}$$

in which

$$\eta_{\rm b} = \widehat{k}\,\widehat{\delta}_{\rm b}, \quad \eta_2 = \widehat{k}\,\widehat{\delta}_2, \quad \widehat{k} = \frac{2}{\Delta\widehat{U}_{\rm b}}. \tag{29}$$

It is not difficult to show that energy conservation is automatically satisfied by the requirement that $H(\psi)$ is the same function of $\psi$ at both stations. Similarly, angular momentum is conserved because $K(\psi)$ is the same function everywhere.

The five equations (16), (17), (21), (24), and (28) were solved using routine NEQNJ in the IMSL library which uses a variant of Newton's method. Elements of the Jacobian matrix were analytically calculated with the help of Mathematica. We initially found it impossible to find a starting guess for the five unknowns that would converge to any solution. To overcome this difficulty, we pretended that the problem was that of a *solid* cylinder of specified radius being pushed through a vortex at a specified speed. Only the first three of the five conditions are then needed and the method readily converged to a solution when starting with an initial guess analytically obtained for the small swirl limit. This converged solution was then substituted into the remaining two conditions (which happen to be linear in $\widehat{T}$ and $\Delta\widehat{p}_{\rm b}$) to obtain the surface tension $\widehat{T}$ and bubble pressure $\Delta\widehat{p}_{\rm b}$ that would make the solution valid for a bubble. Starting with this solution Eve, all the other solutions presented in this paper were obtained by gradually varying parameters and using the previous solution as a starting guess.

Since $U$ always occurs in the combination $U_{\rm b} - U$, the effect of a uniform axial flow on bubble speed is merely additive. The five equations remain unchanged when $\widehat{A}$, $\widehat{B}$ and $\Delta\widehat{U}_{\rm b}$ all change sign. Thus, for every solution that represents a bubble advancing into the vortex, there exists is a solution that represents a bubble withdrawing from the vortex. This is a consequence of time-reversal symmetry of inviscid motion and in practice initial conditions determine the relevant solution.

## 2.2 Free bubble

Consider a cylindrical bubble at time $t$ with finite length $L(t)$ and internal pressure $p_{\rm b}(t)$. If the gas within the bubble remains adiabatic, then

$$p_{\rm b}(t)V^{\gamma}(t) = p_{\rm b0}V_0^{\gamma}, \tag{30}$$

where the subscript '0' denotes initial values. The bubble volume $V(t) \approx \pi\delta_{\rm b}^2(t)L(t)$ if the bubble is long enough that the contribution from its ends is negligible. Writing $p_{\rm b} = p_\infty + \Delta p_{\rm b}$ and $p_{\rm b0} = p_\infty + \Delta p_{\rm b0}$, (30) gives

$$L = \left(\frac{p_\infty + \Delta p_{\rm b0}}{p_\infty + \Delta p_{\rm b}}\right)^{1/\gamma} \frac{V_0}{\pi\delta_{\rm b}^2}. \tag{31}$$

If the acceleration $\partial\mathbf{u}/\partial t$ is small compared to the pressure gradient, say, then one may make the quasi-steady assumption that at each instant, the bubble radius and speed of extension of each end can be obtained from the steady solution at the bubble pressure

implied by (31). We estimate:

$$\frac{\partial \mathbf{u}}{\partial t} \sim \frac{\partial(\Delta U_\mathrm{b})}{\partial t} = \frac{\partial(\Delta U_\mathrm{b})}{\partial L}\frac{\partial L}{\partial t} = 2\Delta U_\mathrm{b}\frac{\partial(\Delta U_\mathrm{b})}{\partial L} = \frac{\partial(\Delta U_\mathrm{b}^2)}{\partial L}, \tag{32}$$

and

$$\nabla P \sim \frac{\rho\Omega^2\delta_1^2}{\delta_1}. \tag{33}$$

In non-dimensional terms therefore, the requirement for quasi-steadiness is:

$$\epsilon_{\mathrm{qs}} \equiv \frac{\left(\partial\Delta\widehat{U}_\mathrm{b}^2\right)}{\partial\widehat{L}} \ll 1. \tag{34}$$

Let us consider two cases for the '0' state: (i) a spherical bubble of radius $R_\mathrm{b}$ in quiescent liquid that is then subjected to the vortex flow field, and (ii) a cylindrical bubble just after the injection device closes. In the first case, $\Delta p_{\mathrm{b}0} = 2T/R_\mathrm{b}$ and $V_0 = (4/3)\pi R_\mathrm{b}^3$. In the second case $\Delta p_{\mathrm{b}0}$ is the reservoir pressure, and $V_0 = \pi\delta_{\mathrm{b}0}^2 L_0$ where $\delta_{\mathrm{b}0}$ is obtained from the steady solution for the given $\Delta p_{\mathrm{b}0}$. Substituting these into (31) we can calculate $L$ corresponding to any solution point of the steady problem. Note that we cannot say anything about the path from the '0' state to the cylindrical one: for instance, a dynamical barrier may exist that prevents the latter from being realized.

# 3 Results

## 3.1 Bubble with specified pressure

Figure 3 displays various results as the relative bubble pressure is varied for different values of the surface tension. Focus first on the propagation speed (graph *a*) and notice that two of the curves (····· and —·— ) have a break near $\Delta\widehat{p}_\mathrm{b} = 0$. This is where the solution algorithm stopped converging either because the solution does not exist or changes too rapidly to track.

Each curve also has a limiting value of $\Delta\widehat{p}_\mathrm{b}$ below which the algorithm also stops converging. We believe these to be genuine limit points beyond which steady solutions do not exist. The presence of a limit point is partially plausible from (1) which shows that the radicand becomes negative if $\Delta\widehat{p}_\mathrm{b}$ is sufficiently large. However,(1) implies that $\Delta U_\mathrm{b} = 0$ at the limit point provided $\kappa$ continues to exist. The fact that the actual limit point occurs for higher $\Delta U_\mathrm{b}$ means that other constraints prevent a solution from existing.

Figure 3*b* plots the vortex radius at station 2 and shows that the vortex pinches instead of being displaced outward by the bubble.

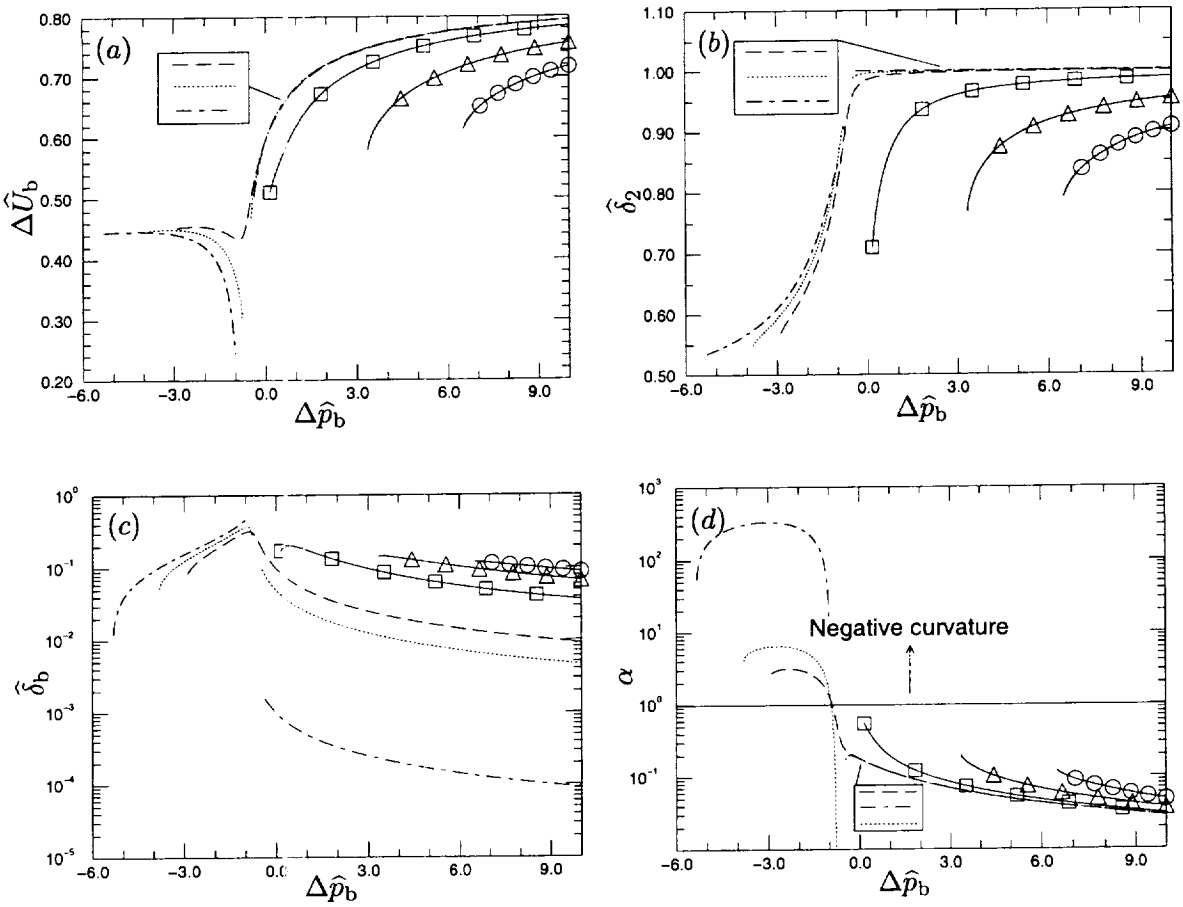


Figure 3: ——— , ○ : $\widehat{T} = 1$; ——— , △ : $\widehat{T} = 0.75$; ——— , □ : $\widehat{T} = 0.40$; - - - : $\widehat{T} = 0.10$; ····· : $\widehat{T} = 0.05$; —·— : $\widehat{T} = 0.001$. (a) Bubble propagation speed $\Delta\widehat{U}_b$. (b) Disturbed vortex radius ($\widehat{\delta}_2$). (c) Bubble radius $\widehat{\delta}_b$. (d) Curvature index $\alpha$ of the bubble tip.

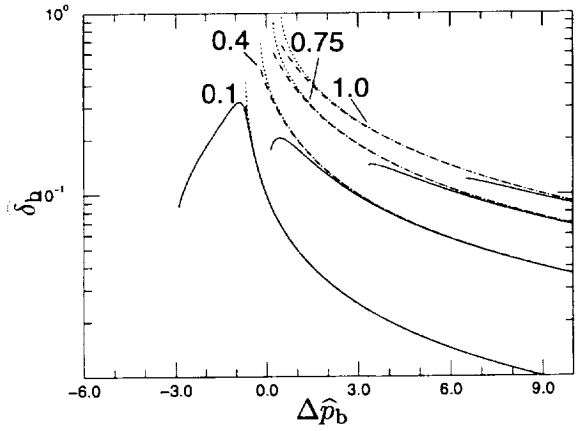


Figure 4: Bubble radius compared approximate formulas. Each curve is labelled with the value of $\widehat{T}$. ——— , exact; ····· , equation (36); - - - - , equation (37).

Figure 3c plots the bubble radius. One may obtain an approximate formulas by supposing that the flow at station 2 is negligibly disturbed relative to the vortex at station 1. The equilibrium radius of a cylindrical bubble in such a flow is given by the condition:

$$p_b - p_1(\delta_b) = T/\delta_b, \tag{35}$$

which, upon using (10), becomes in terms of non-dimensional variables:

$$\Delta\hat{p}_b - \frac{1}{2}\hat{\delta}_b^2 + 1 = \hat{T}/\hat{\delta}_b. \tag{36}$$

An even simpler approximation is obtained by neglecting the term quadratic in $\hat{\delta}_b$:

$$\hat{\delta}_b = \frac{\hat{T}}{\Delta\hat{p}_b + 1}. \tag{37}$$

Figure 4 (dotted) shows that (37) is slightly better than (36) and that both approximations overpredict the exact result implying that the liquid pressure at the bubble radius is smaller than at the same radius in the undisturbed vortex.

Figure 3*d* plots the curvature of the bubble tip as deduced from (1) and the fact that $p_a = p_\infty - \rho\Omega\delta_1^2$. Actually, a curvature index $\alpha$, defined as

$$\alpha \equiv 1 - \kappa\delta_b, \tag{38}$$

is plotted in order to emphasize small difference from $\kappa\delta_b = 1$ on a log scale. A hemispherical nose has $\kappa = 2/\delta_b$ ($\alpha = -1$), a flat tip has $\kappa = 0$ ($\alpha = 1$), while a nose with negative curvature has $\kappa < 0$ ($\alpha > 1$). Figure 3*d* shows that not only is the tip is flatter than hemispherical, i.e., $\alpha > -1$ but $\alpha > 0$. That this should be so is proven as follows. Constancy of the Bernoulli head from the tip to a point on the bubble surface at station 2 gives:

$$p_n = p_2(\delta_b) + \frac{1}{2}\rho u_2^2(\delta_2) = p_b - T/\delta_b + \frac{1}{2}\rho u_2^2(\delta_2), \tag{39}$$

where the fact that the azimuthal velocity is zero on the bubble surface has been used. On the other hand

$$p_n = p_b - \kappa T. \tag{40}$$

Equating (39) and (40) gives $\kappa\delta_b < 1$.

A word of caution: the fact that $\alpha \approx 0$ for large $\Delta\hat{p}_b$ in figure 3*d* should *not* lead one to say that the curvature is approximately known and therefore (1) may be used to approximate the speed. Substituting into (1) the fact that the bubble radius $\hat{\delta}_b \approx \hat{T}/(\Delta\hat{p}_b + 1)$ for large $\Delta\hat{p}_b$ gives:

$$\Delta\hat{U}_b \approx \sqrt{2\alpha\,(\Delta\hat{p}_b + 1)}. \tag{41}$$

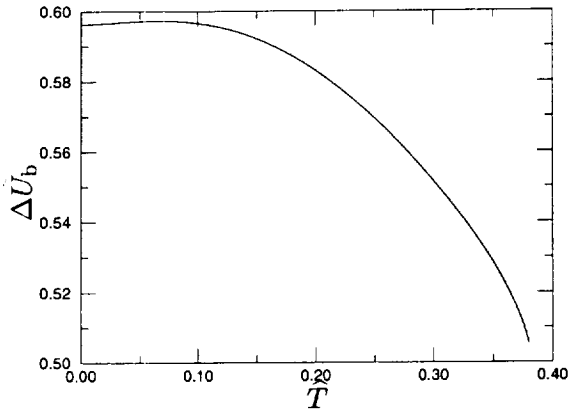


Figure 5: Propagation speed of a bubble at ambient pressure ($\Delta\hat{p}_b = 0$) as a function of surface tension.

Thus for large $\Delta\hat{p}_b$, the speed involves the product of $\alpha$, no matter how small, and a large $\Delta\hat{p}_b$

Note from figure 3*a* that when $\hat{T}$ is small enough, the bubble is able to propagate even when $\Delta\hat{p}_b < -1$, i.e., when bubble pressure is less than minimum vortex pressure. In this case the tip curvature is negative, i.e., the nose is dimpled (figure 3*d*).

The case of $\Delta\hat{p}_b = 0$ is relevant for an unpressurized reservoir and figure 5 plots the speed as the surface tension is varied. Solutions exist for $\hat{T} \leq .380$ which for air and water and a 3 cm core radius corresponds to a modest $\Omega/(2\pi) \geq 0.9$ rev/s.

### 3.2 Free bubble

Here we consider the quasi-steady behavior of a free cylindrical bubble whose pressure and dimensions are compatible with it having initially been a spherical bubble of radius $R_0$ in a quiescent liquid. The parameter space now includes $\hat{R}_0 \equiv R_0/\delta_1$ and $\hat{p}_\infty \equiv p_\infty/(\rho\Omega^2\delta_1^2)$ in addition to $\hat{T}$ and $\Delta\hat{p}_b$. Instead of mapping out the space, we shall be content to sketch three scenarios which we shall denote as A, B1, and B2.

Consider (31) (placing hats on all quantities) as $\Delta\hat{p}_b$ varies. If we begin in the regime $\Delta\hat{p}_b \ll \hat{p}_\infty$, then the first factor in (31) is practically constant as $\Delta\hat{p}_b$ varies. Since, the bubble speed is positive, $\hat{L}$ must increase and therefore $\hat{\delta}_b$ must decrease. Two cases are then possible: the cylindrical bubble may be at a point in figure 3*c* where the $\hat{\delta}_b$ versus $\Delta\hat{p}_b$ curve either has a (A) negative or (B) positive slope.

In the former case, the solution point must move to the right along the curve to allow $\hat{\delta}_b$ to decrease. Thus $\Delta\hat{p}_b$ increases and the elongation continues unabated. The bubble

volume decreases with elongation, however, as long as $\Delta\widehat{p}_b \ll \widehat{p}_\infty$, the decrease is negligible and the bubble will be nearly incompressible. At some point during the elongation, $\Delta\widehat{p}_b$ will become comparable to $\widehat{p}_\infty$. This means that the first factor in (31) will decrease and so $\widehat{\delta}_b$ must decrease faster to allow $L$ to increase. At this stage, the bubble volume will begin to wither away. In fact, when $\Delta\widehat{p}_b \gg \widehat{p}_\infty$ we may use (37) to conclude that the bubble radius will diminish as $\widehat{\delta}_b \sim \widehat{L}^{-2\gamma/(2\gamma-1)} \approx \widehat{L}^{-1.56}$, which is faster than the $\widehat{\delta}_b \sim \widehat{L}^{-1/2}$ behavior of an incompressible bubble.

For case B1, the $\widehat{\delta}_b$ versus $\Delta\widehat{p}_b$ curve has a positive slope. Hence the solution point must move to the left along the curve: $\Delta\widehat{p}_b$ becomes more negative and eventually a limit point is encountered which presumably stops the elongation.

Case B2 is similar to B1 except that the location of the limit point $\Delta\widehat{p}_{b,lim} < -\widehat{p}_\infty$ allows unceasing elongation. As $\Delta\widehat{p}_b$ becomes more negative during the elongation, it will become comparable to $-\widehat{p}_\infty$ at some point. The first factor in (31) then increases and it is no longer necessary for the bubble radius to shrink to allow $L$ to increase. At this point, the bubble radius becomes constant and volume begins to be created indefinitely with bubble pressure becoming arbitrarily close to vacuum.

We now illustrate each of the three cases by means of specific examples.

To demonstrate type A behavior, let us initially have a spherical air bubble of 2 mm radius surrounded by water at atmospheric pressure, that is subjected to a vortex with a 2 cm core rotating at 2 rev/s. These values imply $\widehat{T} = .058$, $\widehat{p}_\infty = 1604$, and $\widehat{R}_0 = 0.1$. The first step is to generate a solution locus for $\widehat{T} = .058$ by varying $\Delta\widehat{p}_b$ as in figure 3. We find that the locus has two branches similar to the dotted curves in figure 3. The present analysis cannot say which branch the bubble will end up on. The left branch exhibits type B1 elongation terminating quickly at $\widehat{L} = 0.39$. The neglect of axial derivatives is unlikely to hold for such a small $\widehat{L}$ (see §4); still behavior with similar characteristics may exist in reality. The right branch exhibits unassailable type A behavior as shown in figure 6: the pressure increases with length and the elongation continues unabated. Figure 6*b* shows that the bubble radius diminishes very nearly as $L^{-1/2}$, i.e., the bubble remains very nearly incompressible. As noted above, we should expect a stage to be reached (when $\Delta\widehat{p}_b > 1604$) where volume diminishes and its existence was verified. The measure of merit, $\epsilon_{qs}$, of the quasi-steady assumption, decreases from 0.2 to 0.004 in the range of figure 6.

To depict type B elongation, let us choose $\widehat{T} = 0.001$ (see chain-dot curves in figure 3). This is achieved by increasing $\Omega/(2\pi)$ to 15.18 rev/s, leaving all other dimensional parameters the same as in the previous example. We then have $\widehat{p}_\infty = 27.83$. Again, the solution locus has two branches. The right-hand branch (type A) is found to start at $\widehat{L} \approx 500$ and

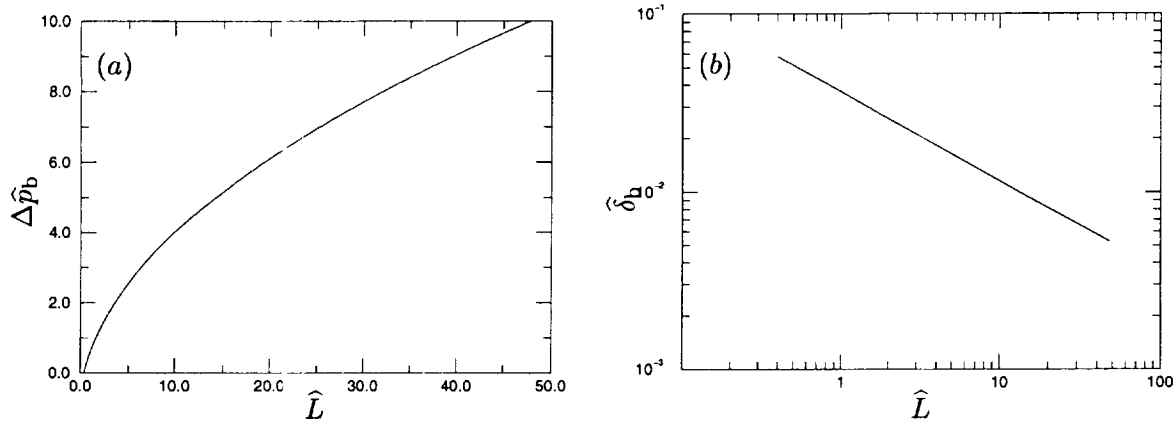


Figure 6: Evolution of bubble pressure and radius with elongation (example illustrating case A).

one cannot rule out an unsteady process that somehow produces such a cylindrical bubble. Let us focus on the left-hand branch (type B). Figure 7*a* shows that the bubble pressure decreases as the bubble elongates, and a limit point is suddenly encountered. The curves were truncated at the left in order that the acceleration parameter $2 \times 10^{-5} \leq \epsilon_{qs} \leq 0.1$ in the range of the plot. Again, quasi-steadiness becomes a better approximation as the bubble extends.

Finally, to obtain type C behavior, let us choose $\Omega/(2\pi) = 10$ rev/s, $\delta_1 = 7$ cm and $R_0 = 3$ mm. We then have $\hat{T} = 5.4 \times 10^{-5}$, $\hat{p}_\infty = 5.24$, and $\hat{R}_0 = .043$. The right branch (type A) begins at an absurd $\hat{L} \approx 14,000$ and so we focus on the left branch which begins at a reasonable state. The limit point of the left branch lies at $\Delta\hat{p}_{b,lim} \approx -5.42 < -\hat{p}_\infty$ thus allowing unabated elongation together with creation of volume. Figure 8*a* shows that the bubble radius initially decreases and then becomes constant as seen in stages III and IV of the experiments [3]. The bubble pressure, shown in figure 8*a* , becomes nearly constant as the bubble elongates. This means that the bubble speed becomes nearly constant and the acceleration parameter becomes ever smaller; it decreases from 0.1 to $10^{-7}$ in the range of the plot.

# 4 Closing remarks

Using a method introduced by Batchelor [2], the speed of propagation of a semi-infinite cylindrical bubble into a vortex has been calculated without knowning the shape of the nose and found to be comparable to the maximum rotational speed in the vortex.

If the pressure in the reservoir is indeed constant in time, then the main assumption

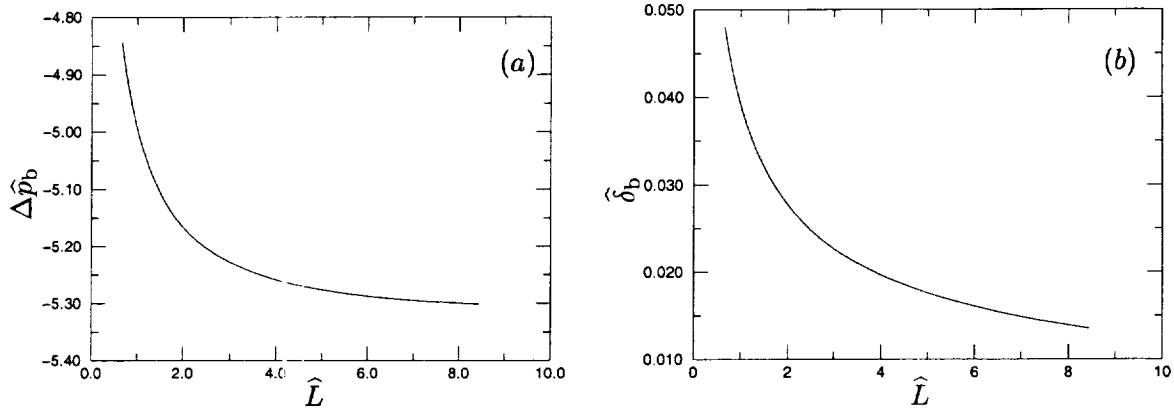


Figure 7: Evolution of bubble pressure and radius with elongation (example illustrating case B1).

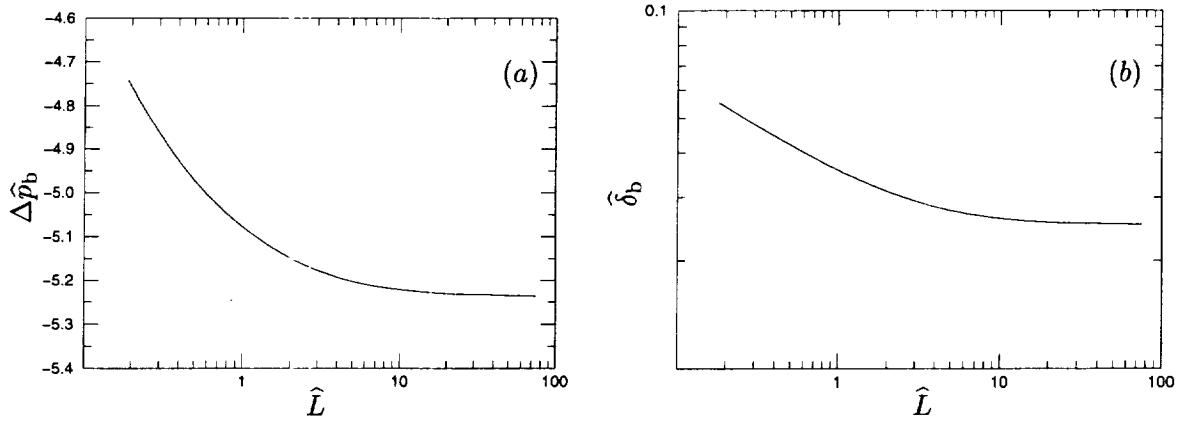


Figure 8: Evolution of bubble pressure and radius with elongation (example illustrating case B2).

in the present treatment is that of a semi-infinite bubble. This allows neglect of axial derivatives at station 2. How valid is this for a finite bubble of length $L$?. Since the axial velocity must vanish at the axial center of the bubble, axial derivatives of velocity $\sim U_b/L$. On the other hand, radial derivatives of velocity $\sim \Omega$ hence axial derivatives are small provided $\widehat{U}_b/\widehat{L} \ll 1$. Since the numerical results showed that $\widehat{U}_b = \mathcal{O}(1)$, the requirement is that $\widehat{L} \gg 1$.

Using the assumption of quasi-steadiness, we applied the constant pressure solution to bubbles with variable pressure. The validity of the assumption can be checked *a posteriori* for each case by calculating the characteristic acceleration (34). Depending on physical parameters and initial conditions, three distinct cases are possible. They are summarized in the abstract.

Let us list the most salient of the many questions that remain unanswered:

(1) What happens when one tries to inject a fixed pressure bubble at a point $\left(\Delta\widehat{p}_b, \widehat{T}\right)$ in the parameter space beyond a limit point? In a similar vein, what happens when a quasi-steady variable pressure bubble arrives at a limit point in scenario B1.

(2) What is the status of the gaps in figure 3?

(3) The present work assumes that one already has a cylindrical bubble. What conditions make possible the evolution from a spherical to a cylindrical bubble? What determines whether the solution will end up on a type A or type B1/B2 trajectory.

(4) A uniform axial velocity in the vortex cores merely adds to the velocity of bubble propagation. It would be useful to implement the present procedure (numerically) for more general profiles perhaps in conjunction with an experiment that injects air into a vortex ring or into the vortex of an airfoil in a water tunnel or towing tank.

(5) The stability of a cylindrical bubble surrounding by a purely circumferential flow has been studied by Pedley [6], for instance. The result is that the surrounding flow stabilizes the bubble. In the present situation the flow at station 2 also includes an axial flow. What are the stability properties of the station 2 flows?

**Acknowledgement**

We are grateful to Dr. Meng Wang for a very useful discussion prior to which we erroneously believed that momentum conservation was implied by the rest of the conditions.

## References

[1] Marten, K., Shariff, K., Psarakos, S. & White, D.J., "Ring bubbles of dolphins," Scien-

tific American, August 1996, pp. 83–87.

[2] Batchelor, G.K., *An Introduction to Fluid Dynamics.* Cambridge University Press (1967).

[3] Maines, B.H. & Arndt, R.E.A., "Bubble dynamics of cavitation inception in a wing tip vortex," In *Cavitation and Multiphase Flow Forum - 1993* (ed. O. Furuya), pp. 93–97, Fluids Engineering Division, vol. 153, ASME, (1993).

[4] Gradshteyn, I.S. & Ryzhik, I.M. *Table of Integrals, Series, and Products.* Academic (1980).

[5] Watson, G.N., *A Treatise on the Theory of Bessel Functions.* Macmillan (1944).

[6] Pedley, T.J., "The stability of rotating flows with a cylindrical free surface," *J. Fluid Mech.* **30**, 127–147, (1967).